

ARTICLE

<https://doi.org/10.1038/s42004-019-0138-z>

OPEN

Synthesis of super bright indium phosphide colloidal quantum dots through thermal diffusion

Mitchell T. Clarke¹, Francesco Narda Viscomi², Thomas W. Chamberlain ³, Nicole Hondow⁴, Ali M. Adawi ^{2,5}, Justin Sturge ¹, Steven C. Erwin⁶, Jean-Sebastien G. Bouillard ^{2,5}, Sudarsan Tamang⁷ & Graeme J. Stasiuk ¹

Indium phosphide based quantum dots have emerged in recent years as alternatives to traditional heavy metal (cadmium, lead) based materials suitable for biomedical application due to their non-toxic nature. The major barrier to this application, is their low photoluminescent quantum yield in aqueous environments (typically < 5%). Here we present a synthetic method for InP/ZnS quantum dots, utilizing a controlled cooling step for equilibration of zinc sulfide across the core, resulting in a photoluminescent quantum yield as high as 85% in organic solvent and 57% in aqueous media. To the best of our knowledge, this is the highest reported for indium phosphide quantum dots. DFT calculations reveal the enhancement in quantum yield is achieved by redistribution of zinc sulfide across the indium phosphide core through thermal diffusion. By eliminating the need for a glove box and relying on Schlenk line techniques, we introduce a widely accessible method for quantum dots with a realistic potential for improved biomedical applications.

¹ Department of Biomedical Sciences, University of Hull, Cottingham Road, Hull HU6 7RX, UK. ² Department of Physics and Mathematics, University of Hull, Cottingham Road, Hull HU6 7RX, UK. ³ Institute of Process Research and Development, School of Chemistry, University of Leeds, Leeds LS2 9JT, UK. ⁴ School of Chemical and Process Engineering, University of Leeds, Leeds LS2 9JT, UK. ⁵ G. W. Gray Centre for Advanced Materials, University of Hull, Cottingham Road, Hull HU6 7RX, UK. ⁶ Center for Computational Materials Science, Naval Research Laboratory, Washington, DC 20375, USA. ⁷ Department of Chemistry, School of Physical Sciences, Sikkim University, Tadong 737102, India. Correspondence and requests for materials should be addressed to G.J. S. (email: g.stasiuk@hull.ac.uk)

Colloidal semiconductor nanocrystals (NCs), also known as quantum dots (QDs), have gained significant research interest since the seminal work published >30 years ago^{1–5}. QDs possess unique photoluminescent qualities that can be adjusted with changes to their physical properties such as size, shape, composition and surface state⁶. QDs have fundamental and technical application in light-emitting diodes⁷, optoelectronic devices⁸, energy conservation⁹ and biomedical imaging¹⁰, due to their unique size-dependent properties^{6,11–13}. In an effort to develop Cd-free QDs, alternative materials have been explored, within the II–VI¹⁴ and III–V¹⁵ semiconductor families. In particular, the non-toxic and environmentally friendly indium phosphide (InP) has garnered interest and become one of the most widely investigated semiconductors in colloidal NCs. InP is a III–V semiconductor with a bulk bandgap energy of 1.35 eV and an exciton Bohr radius of the order of 10 nm, therefore allowing for the synthesis of NCs with emission wavelength covering the entire visible range¹⁶, from blue ($\lambda_{em} = 480$ nm) to near-infrared ($\lambda_{em} = 750$ nm)¹⁵. This wide tunability, combined with inherent non-toxicity (heavy metal free), make InP-based QDs strong candidates for use within a biological setting¹⁷. When InP/ZnS QDs were intravenously injected into mice, there were no visible signs of toxicity observed over a 12-week duration¹⁸. Likewise Brunetti and Chibli have independently demonstrated the increased toxicity of Cd²⁺ compared to In³⁺^{19,20}.

In the absence of a protective shell, InP QDs typically exhibit a poor photoluminescent quantum yield (PLQY) of <1%²¹, which is attributed to the surface trap states of the core InP NCs. Etching of the QD surface using hydrogen fluoride has shown to increase PLQY values to 30%²¹. Surface passivation using an inorganic shell has improved PLQY values up to 60% in organic solvents^{22,23}. With a bandgap of 2.26 eV, a valence band edge at 3.61 eV and a lattice mismatch of only 8% with InP, zinc sulphide (ZnS) is an ideal shell material for InP QDs^{15,24}. Accordingly, InP/ZnS have emerged as the most commonly synthesised InP-based core/shell QDs. The relatively low lattice mismatch between InP and ZnS allows for the growth of ZnS monolayers on the core surface rather than independent formation of ZnS NCs within the reaction mixture.

The PLQY of InP/ZnS QDs can increase to 50–75% in organic media^{22,25,26}. This increase in PLQY enables InP/ZnS QDs to be used for biomedical imaging, albeit with a strong dependence on the phase transfer to aqueous phase maintaining at least 40% of the original PLQY. A range of thiol-containing ligands including thioglycolic acid (TGA) have been reported to yield InP/ZnS core/shell QDs capable of maintaining up to 42% of their original PLQY, with Tamang et al. showing an efficient ligand exchange method on the ZnS surface²⁷. Increasing PLQY values of QDs following their transfer to aqueous solvent/media is a critical step in the pathway to enhanced biomedical imaging and sensing.

Here we show a synthetic method for the passivation of defect states in InP core QDs with redistribution of ZnS via thermal diffusion across the core surface that creates greater shell

coverage. The resultant InP/ZnS core/shell QDs have an enhanced PLQY of 85% in organic media and 57% in aqueous media. This is the highest PLQY that has been reported to date for InP/ZnS QDs.

Results

Synthesis and characterisation of InP and InP/ZnS(1) QDs.

Synthesis of the InP core requires the use of both Zn²⁺ and In³⁺ precursors (in this case an InCl₃) in a primary amine. It has also been demonstrated that the use of different In³⁺ halide precursors results in different specific emission profiles, ranging from 525 to 620 nm (from green to red, respectively)²³. The reaction occurs in oleylamine that acts as a solvent and surface ligand for InP core growth. The properties of oleylamine also allow for reaction temperatures in excess of 300 °C without decomposition. The Zn²⁺ precursor (ZnCl₂) is used in the initial reaction solution to passivate surface defects and trap states during InP core growth²⁸. This method employs tris(dimethylamino)phosphine (P(DMA)₃) to allow for the synthesis to be conducted without fatty acid ligands containing silylphosphines that can cause surface oxidation even under strictly air-free conditions²⁹. The use of aminophosphines such as P(DMA)₃ opens the door for Schlenk line techniques to be used in place of glove box-based methods to synthesise InP core only QDs. Additionally, ZnS shells as thick as 10 nm have been grown around InP cores using an aminophosphine route³⁰. This is attributed to the absence of the thin oxide layer on the InP surface that typically impedes shell growth. The formation of the InP cores was completed following hot injection of P(DMA)₃, the reaction then reaches completion within 30 min, with growth of the InP cores being accurately followed by ultraviolet–visible (UV-Vis) spectroscopy (Supplementary Figure 1). On completion of core growth, the addition of ZnS was achieved by initially adding a chalcogen precursor. Trioctylphosphine saturated with sulphur (TOP-S) is used instead of dodecanethiol (DDT), a precursor often employed for monolayer growth, due to the fact that hypsochromic shifts in emission maxima measurements are not observed when using TOP-S. The shifts to shorter wavelength that are observed when using DDT are attributed to surface etching of InP²⁸. The introduction of TOP-S is followed by the addition of Zn²⁺ precursor (Zn-stearate) in 1-octadecene. Further addition of Zn²⁺ is required owing to the limiting amount of Zn²⁺ precursor initially added during the core formation step.

The InP cores have an average diameter of 2.48 nm (Table 1, Fig. 1), which were attained after 30 min from InCl₃, which is within the size range previously reported²³. After growth of a ZnS shell, the emission maximum for **InP/ZnS(1)** was observed at $\lambda_{em} = 613$ nm with a full width at half maximum of 52 nm (Fig. 2a) and a PLQY of 40–49% in hexane (Table 1). Transmission electron microscopy (TEM) images of **InP** and **InP/ZnS(1)** QDs show that the average particle size increases from 2.48 to 2.67 nm upon addition of the ZnS shell with an

Table 1 Physical and photophysical properties of red-emitting QDs in hexane

QD	Zn:In ratio ^a	Diameter ^b (nm)	λ_{em} (nm)	PLQY Φ	Lifetime (ns)	Γ_{rad} (ns ⁻¹)	$\Gamma_{non-rad}$ (ns ⁻¹)
InP	37:63 (± 1.27)	2.48 \pm 0.45	—	—	—	—	—
InP/ZnS(1)	57:33 (± 1.36)	2.67 \pm 0.48	613	49%	19.7	0.025	0.026
InP/ZnS(2)	73:27 (± 0.28)	2.75 \pm 0.45	623	85.30%	20.5	0.042	0.007
InP/ZnS(3)	89:11 (± 0.11)	2.88 \pm 0.49	611	47%	22.1	0.021	0.024

PLQY photoluminescent quantum yield, QD quantum dot

^aSemi-quantitative energy-dispersive X-ray analysis, taken as an average of multiple areas with the standard deviation of the measurements shown in brackets

^bMeasured from transmission electron microscopy images

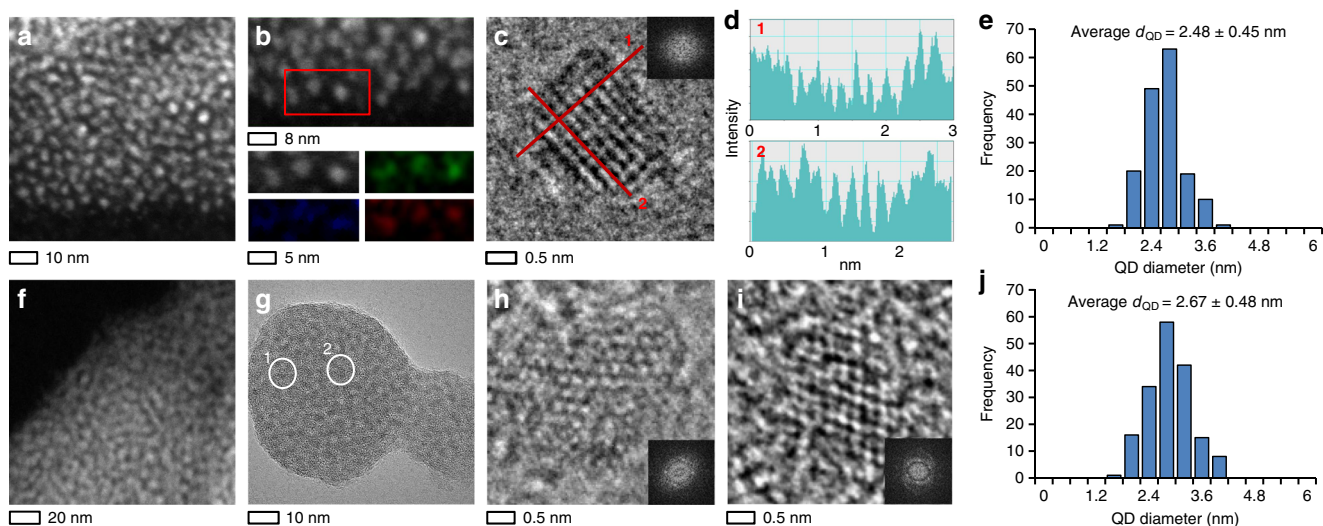


Fig. 1 Physical properties of InP cores (a–e) and traditionally synthesised InP/ZnS(1) quantum dots (QDs) (f–j). **a, b** Scanning transmission electron microscopy (STEM) images and energy-dispersive X-ray mapping confirming the presence of Zn (red), P (blue), and In (green), **c** transmission electron microscopy (TEM) image of an individual QD and **d** corresponding line profiles and **e** size distribution of the InP core. Wide field of view **f** STEM and **g** TEM images, **h, i** TEM images of individual QDs 1 and 2 (circled in **g**, fast Fourier transforms inset) and **j** size distribution of InP/ZnS(1) QDs

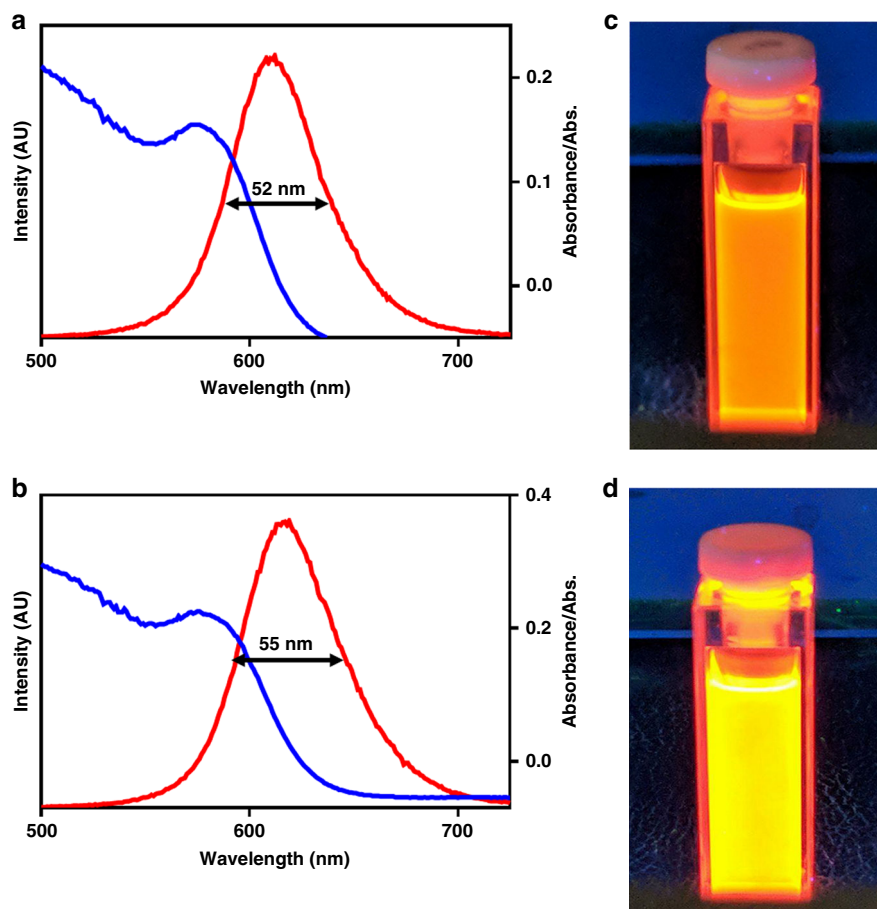


Fig. 2 Photophysical properties of InP/ZnS(1) and InP/ZnS(2). **a, b** Absorption (red) and emission spectra (blue), along with the full width at half maximum InP/ZnS(1) (a) and InP/ZnS(2) (b). **c, d** Photographs showing the obtained luminescence of both InP/ZnS(1) (c) and InP/ZnS(2) (d) under ultraviolet light (365 nm)

increased Zn:In ratio of 57:43 (Table 1) shown by energy-dispersive X-ray (EDX) spectroscopy (Supplementary Figure 2). The crystalline nature of the QDs was confirmed via fast Fourier transforms (FFTs) of the lattice images, with the Fourier pattern consistent with the cubic zinc blende phases of InP and InP/ZnS (1), confirmed by X-ray powder diffraction (Supplementary Figure 3)³¹.

Synthesis of InP/ZnS(2) by thermally controlled cooling. Significantly, InP/ZnS QDs formed using a thermal controlled cooling phase followed by a second successive heating method exhibit significantly enhanced PLQY (Table 1). This method involves cooling of InP/ZnS(1) to 180 °C under argon, followed by a second precursor injection of ZnS and incremental heating to 240 °C as seen in the formation of InP/ZnS(1). This second injection step results in an overall increase in size from 2.67 to 2.75 nm with an increase in Zn:In ratio of 57:43–73:27 (Table 2, Fig. 3). The InP/ZnS QDs that have undergone this second procedure, (InP/ZnS(2)), have a greatly improved PLQY compared to InP/ZnS(1) with a PLQY of 49%, while InP/ZnS(2) have a PLQY ranging from 75% to as high as 85.3% in hexane. This is the highest PLQY observed for InP/ZnS-based QDs to date, as shown in Fig. 2.

In comparison to other work carried out using aminophosphine-based precursors, this is the highest reported PLQY in organic solvent. Previously, Hines and co-workers achieved a PLQY of up to 60% with the same precursor and Deng et al. achieved 76.1% when

synthesising blue-emitting InP QDs^{23,26}. The higher PLQY level following this successive heating synthesis method, when compared to traditional methods, is attributed to an increase in the passivation of defect sites on the core with ZnS, leading to a reduction in the number of non-radiative decay pathways (Table 1). To look at the difference between the two methods (traditional and successive), quantification of the shell thickness in each case was performed by expressing the thickness in terms of monolayers of ZnS²⁴. TEM measurements indicate an increase in particle size, which is assumed to be ZnS, from which it is possible to calculate the number of monolayers based on the average increase in diameter.

$$V_s = V_{cs} - V_c \quad (1)$$

$$V_s = \frac{4}{3}\pi(r + xd)^3 - \frac{4}{3}\pi r^3 \quad (2)$$

Assuming that the InP cores are spherical with a radius (r in nm), then the volume of the ZnS shell (V_s in nm³) can be derived by the difference in the volume of the InP/ZnS core/shell (V_{cs}) and the volume of the InP core (V_c), as explicitly shown in Eqs. 1 and 2, where x is the number of ZnS monolayers and d is thickness of one monolayer. Using the well-known thickness of one monolayer of a ZnS, 0.32 nm³², and the QD diameters shown in Table 1, it can be shown that 0.391 and 0.513 ZnS monolayers were added onto the surface of the core for InP/ZnS(1) and InP/ZnS(2), respectively.

Density-functional theory calculations. Computational modeling of the factors governing the evolution of InP/ZnS QD shapes gives additional insight into the observed increase in PLQY. We assume that the initial growth stage of the ZnS shell takes place in the kinetic regime, meaning that activation barriers to surface diffusion cannot be overcome and therefore thermodynamic equilibrium is not reached. DFT calculations reveal a strong preference for Zn atoms to bind to ZnS (the adsorption energy is 2.7 eV on the (001) surface) compared to InP (1.9 eV). This preference means that the first layer of Zn shell will tend to nucleate on ZnS, if it is present, rather than on InP. This expectation is consistent with our observation of irregularly

Table 2 Photophysical properties of InP/ZnS(1) and InP/ZnS(2) in H₂O

QD	PLQY ϕ	Lifetime (ns)	
InP/ZnS(1)-TGA	20%	15.3 (52.82%)	1.4 (47.18%)
InP/ZnS(2)-TGA	57.09%	17.6 (72.38%)	0.7 (27.62%)

PLQY photoluminescent quantum yield, QD quantum dot

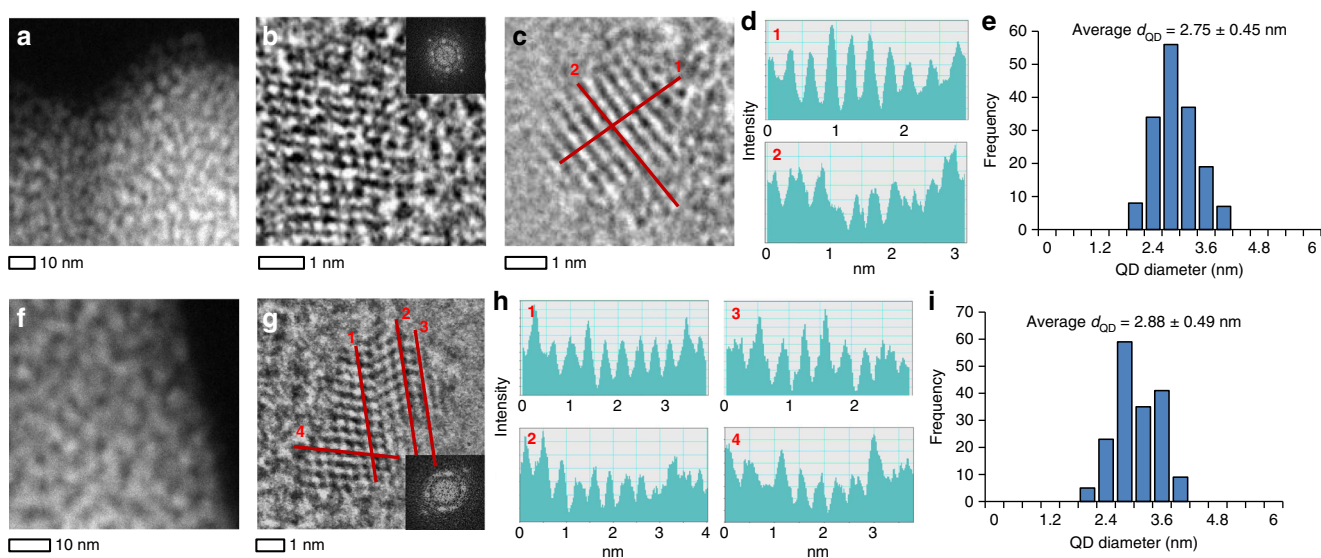


Fig. 3 Physical properties of InP/ZnS(2) (a–e) and InP/ZnS(3) quantum dots (QDs) (f–i) highlighting the crystalline nature of the QDs. **a** Scanning transmission electron microscopy (STEM) image, **b, c** transmission electron microscopic (TEM) images of individual QDs (fast Fourier transforms (FFTs) inset) and **d** corresponding line profiles and **e** size distribution of InP/ZnS(2). **f** Wide field of view STEM image, **g** TEM image of an individual QD (FFT inset) and **h** the corresponding line profiles and **i** size distribution of InP/ZnS(3)

shaped, asymmetric QDs with bare InP patches and small islands of ZnS located sporadically on the surface (TEM images in Fig. 1h). However, given sufficient time, these irregularly shaped QDs will eventually relax towards their equilibrium shape. For ZnS, this shape is bounded entirely by (110) facets³³. The time-scale for this relaxation process is determined by the energy barriers for surface diffusion of Zn and S atoms on ZnS.

These barriers are well defined for the (110) facets. DFT nudged-elastic band calculations gives their values as 0.69 eV for Zn atoms and 0.75 eV for S atoms (Fig. 4). Such modest barriers are easily surmounted at the temperatures used in our experiments, and therefore the equilibrium shape can indeed be reached on laboratory time scales.

The resulting physical picture then is that, when growth is restarted, the small ZnS islands redistribute themselves over the surface, leading to a conformal quasi-spherical core/shell QD (Figs. 3b and 4), which results in an increased PLQY. Therefore, the cooling phase prior to the second addition of Zn and S precursors plays a major role in increasing ZnS coverage of the InP core. Decreasing non-radiative decay pathways leads to increases in PLQY to as high as 85% in organic phase for InP/ZnS(2).

Synthesis and characterisation of InP/ZnS(3) QDs. To validate our successive heating synthesis approach, a QD control was

formed using a traditional single heating method with double the concentration of Zn and S precursors added to the InP cores to form InP/ZnS(3) (Fig. 3). InP/ZnS(3) shows a Zn:In ratio of 89:11 with a diameter of 2.88 ± 0.49 nm and using Eqs. 1 and 2 can be shown to have 0.715 monolayers of ZnS. The size of the InP/ZnS(3) was shown to be similar to the InP/ZnS(2), but the Zn content was greater. Therefore, the Zn content is not the cause of the PLQY enhancement as InP/ZnS(3) shows a PLQY of 47% (Table 1), which is more comparable to the traditionally synthesised QDs (cf. InP/ZnS(1) = 49%). Lifetime measurements for all the QDs in hexane from all three methods show a single exponential decay corresponding to an excited lifetime in a similar range of 20 ns (Table 1). InP/ZnS(2) shows a suppression of non-radiative decay pathways, suggesting greater passivation of the core using the successive method (Table 1). The observed increase in the PLQY for InP/ZnS(2) is not only attributed to higher zinc content but also to the thermally activated diffusion of the first ZnS layer to an equilibrium state, which coats a larger amount of the surface of the core (Fig. 4). This increased coverage provides greater insulation to the core against the decay processes from holes and solvent-quenching effects. If allowed to continually grow in one step, the ZnS will not cover as much of the core as it favours ZnS island formation and the high concentration of Zn and S has less of an effect on the PLQY of the resultant QDs (Supplementary Figures 4–8).

Aqueous phase studies of InP/ZnS (1 and 2). The PLQY of the InP/ZnS(2) in hexane was enhanced to a value in excess of 80%. However, for use within a biological setting phase transfer to an aqueous solution must be undertaken. A purified sample of QDs in chloroform underwent phase transfer into aqueous solution using TGA as the transfer ligand (Supplementary Figures 9–11). PLQY of InP/ZnS(2) in water was shown to have values of 57% (Table 2), which is significantly higher than previously reported InP/ZnS QDs in aqueous media.

Enhancement in the PLQY in aqueous solution will allow InP-based QDs to be used in more biomedical imaging applications as the PLQY is comparable to that of toxic heavy metal QDs (Cd based)³⁴. Lifetime measurements in water show two decay pathways (Table 2), a slow and a fast component. The slow component is in the range of 15–17 ns, similar to the hexane decay pathway, and the fast component is between 0.7 and 1.4 ns, indicating a decay pathway via H₂O solvent oscillators (Table 2). The weighting between fast and slow component switches depending on the ZnS coverage. For InP/ZnS(1), the fast component is 1.413 ns with a weighting of 47.18%, and for InP/ZnS(2), 0.708 ns at a 27.62% weighting, illustrating a lower solvent quenching by H₂O solvent oscillators with InP/ZnS(2). This results in an increase in weighting of the slow component in InP/ZnS(2) directly corresponding to higher PLQY. Using this technique, InP/ZnS(2)-TGA can now be a viable replacement to the Cd-based QDs in biological imaging. Longitudinal studies of InP/ZnS(2) in aqueous solutions, over a period of 7 days (Fig. 4), shows that at least 68% of the initial PLQY was retained. The stability of QD-TGA-capped QDs in water represents a more than adequate ‘shelf life’ for their application in biological settings.

Discussion

A synthetic method for the enhancement of PLQY in non-toxic InP/ZnS-based QDs has been developed. This method eliminates the need for a glove box, relying only on Schlenk line techniques, and produces QDs that exhibit a PLQY as high as 85% in organic solvent. After phase transfer to aqueous media, the PLQY is 57%, which is significantly greater than any previously reported. The

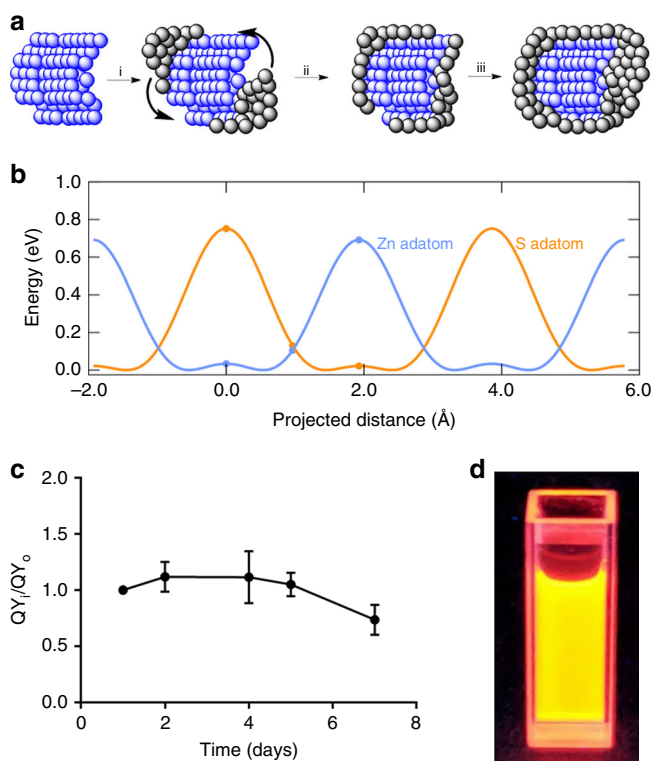


Fig. 4 Shell formation on InP/ZnS(2) and photophysical properties in water. **a** Scheme showing proposed growth mechanism of the quantum dots (QDs): (i) initial shell growth, (ii) thermal equilibrium of ZnS across core, and (iii) further growth of shell. **b** Shows the potential surface energy for the diffusion of the ZnS atoms across the surface of the InP core. **c** The mean photoluminescent quantum yield (PLQY) over a 7-day period for InP/ZnS(2) QDs capped in thioglycolic acid (TGA) in aqueous solution, where QY_0 is the PLQY immediately after phase transfer and QY_i is the PLQY on i days later (error bars are SD $n = 3$). **d** Photographs showing the obtained luminescence of InP/ZnS(2)-capped TGA in aqueous solution

additional cooling phase in this method was shown to induce thermally activated diffusion of the ZnS shell to an equilibrium state. This allows for significantly larger coverage of the InP core, leading to greater quantum confinement of excitons, and increased protection from highly quenching aqueous solvents. In contrast, the traditional shell growth method leads to ZnS island formation on the surface of InP cores resulting in lower coverage and lower PLQY. This method allows for increased PLQY in aqueous solutions, therefore opening a wider scope of biomedical applications for the non-toxic InP-based QDs. Further, the thermal equilibrium method of shell growth discussed in this paper could have great importance for many other core/shell systems.

Methods

Reagents. Reagents were received in the following purities and used without further purification: 99.999%—Indium chloride (Alfa Aesar), indium iodide (Alfa Aesar) and zinc chloride (Sigma-Aldrich); 90%—sulphur powder (Sigma Aldrich) and D-penicillamine (Alfa Aesar); 97%—tris(diethylamino)phosphine, trioctylphosphine (Sigma-Aldrich) and tetramethylammonium hydroxide solution (Sigma-Aldrich); 90%—1-octadecene technical grade (Sigma-Aldrich); 70%—oleylamine technical grade (Sigma-Aldrich); phosphate-buffered saline (PBS; 1×, pH 7.4) (Gibco); tris(2-carboxyethyl)phosphine hydrochloride solution (0.5 M pH) (Sigma-Aldrich).

Instruments. TEM was undertaken on a FEI Titan³ Themis G2 operating at 300 kV fitted with 4 EDX silicon drift detectors and a Gatan One-View CCD. Bruker Esprit software (Version 1.9.4) was used for EDX spectra collection and analysis. High-angle annular dark field scanning TEM (STEM) and EDX mapping were conducted using a probe current of ~150 pA. Samples were prepared for TEM by placing a drop of suspended QDs on a graphene oxide-coated holey carbon film supported on a copper TEM grid (EM Resolutions, UK). QD sizing was performed by measuring the diameter of a statistically relevant number of individual QDs (~150 QDs per sample) in the STEM images.

Fluorescent measurements. All fluorescent measurements were completed using a Horiba Fluoromax-4P spectrofluorometer in a 10 mm quartz cuvette. All spectra were taken in either aqueous or hexane solutions dependent on whether QDs had undergone phase transfer. All UV-Vis absorption spectra were recorded on a thermoscientific Evolution 300. Fluorescence quantum yields were determined by comparison of the integrated fluorescent intensity of QDs against the integrated standard (blanks were used as integrated standards—hexane (organic) milli-Ω water (aqueous)), using an integration sphere. All samples (including blanks) were excited at 405 nm for spectra to be produced in QY measurements (Supplementary Note 1).

The lifetime was measured in a 10 mm quartz cuvette. Excitation was at 405 nm and emission was collected at 612 nm using a Becker and Hickl HPM-100 detector.

Synthesis of InP cores. InCl₃ (0.45 mmol) and Zn(II) chloride (300 mg, 2.2 mmol) were added to oylamine (5.0 mL, 15 mmol). The reaction mixture was stirred and degassed for a minimum of 30 min at 120 °C. Following this, the reaction mixture was backfilled with Ar and heated to 180 °C (and the temperature was allowed to stabilise before progressing with the reaction). After 10 min, tris(dimethylamino) phosphine (0.45 mL, 1.6 mmol) was rapidly injected. On injection of the phosphine precursor, the reaction occurred rapidly with core-only InP QDs formed within 30 min. On completion, the reaction was brought down to room temperature and core-only InP QDs were precipitated in ethanol (50 mL) before being re-suspended in organic solvent (hexane).

Synthesis of InP/ZnS(1) core/shell QDs. After 20 min, a saturated TOP-S solution (1 mL of a 2.2 M solution) was injected slowly to a solution of InP cores at 180 °C. After 60 min, the temperature is increased from 180 to 200 °C. After 120 min, a solution of Zn(stearate)₂ (1 g) in 1-octadecene (ODE) (4 mL) was injected slowly. The temperature was then increased from 200 to 220 °C. After 150 min, TOP-S (0.7 mL of a 2.2 M solution) was injected slowly. The temperature was then increased from 220 to 240 °C. After 180 min, a solution of Zn(stearate)₂ (0.5 g) in ODE (2 mL) was injected slowly. The temperature was then increased from 240 to 260 °C. After 210 min, the reaction was complete and the solution was brought down to room temperature and InP/ZnS(1) QDs were precipitated in ethanol (50 mL) before being re-suspended in organic solvent (hexane).

Synthesis of InP/ZnS(2) core/shell QDs. On completion of reaction for InP/ZnS(1), the reaction mixture containing InP/ZnS(1) QDs was cooled to 180 °C and temperature allowed to stabilise for 20 min. Following this saturated TOP-S (1 mL of a 2.2 M solution) was injected slowly. After 30 min the temperature was

increased from 180 to 200 °C. After 90 min a solution of Zn(stearate)₂ (1 g) in ODE (4 mL) was injected slowly. The temperature was then increased from 200 to 220 °C. After 120 min TOP-S (0.7 mL of a 2.2 M solution) was injection slowly. The temperature was then increased from 220 to 240 °C. After 150 min a solution of Zn(stearate)₂ (0.5 g) in ODE (2 mL) was injected slowly. The temperature was then increased from 240 to 260 °C. After 180 min the reaction was complete and the solution was brought down to room temperature and InP/ZnS(2) QDs were precipitated in ethanol (50 mL) before being re-suspended in organic solvent (hexane).

Phase transfer of InP/ZnS(2). Phase transfer was completed following a procedure previously reported by Tamang et al.²⁷.

Purification. InP/ZnS(2) QDs first undergo a thorough purification to remove any hydrophobic ligands. A 5 mL solution containing QDs in organic solvent is mixed with anhydrous ethanol (1:3) and centrifuged at 10,000 rpm for 6 min. The pellet is then re-suspended in a chloroform:ethanol (1:3) solution before being centrifuged again at 10,000 rpm for 6 min. On completion, the pellet is then resuspended in minimum amounts of chloroform. For a typical phase transfer of QDs from organic to aqueous solution, a 0.2 M solution of D-penicillamine or thioglycolic acid ligand is prepared in degassed Milli-Q water (1 mL, 8 MΩ), and the pH is adjusted to pH 9 by dropwise addition of 0.5 M tetramethylammonium hydroxide. This solution is mixed with an ~5 μM dispersion of the QDs in chloroform (1.5 mL). The biphasic mixture is stirred vigorously at 1400 rpm for as long as 2 h. On completion, the biphasic mixture can result in a clear separation of two distinct layers or in an emulsion. If the latter is the case, the mixture is centrifuged at low speed (1000 rpm) for 1 min to obtain a separation of two phases. QDs in the aqueous phase will be in the upper phase of the two. QDs in aqueous phase were centrifuged in a Millipore centrifuge filter (VWR) (30 KD) at 6000 rpm for 2 min. Then 200 μL of 1× PBS buffer (pH 7.4) or milli-Q water is used to redisperse the pellet and the sample is stored in the dark at 4 °C.

DFT calculations. First-principles total-energy calculations were used to determine activation barriers for the surface diffusion of Zn and S atoms on ZnS(110). The calculations were performed in a slab geometry with five atomic layers and a vacuum region of 10 angstroms. We considered diffusion along (1–10) and, for each adsorbate position along the path, relaxed all atomic positions in the top two layers until the largest force component on every atom was <0.05 eV/angstrom. Total energies and forces were calculated within the generalised-gradient approximation of Perdew, Burke, and Ernzerhof to DFT using projector-augmented wave potentials, as implemented in VASP³⁵. The plane-wave cut off for all calculations was 280 eV.

Data availability

The authors declare that the data supporting the findings of this study are available within the paper and its supplementary information files.

Received: 30 October 2018 Accepted: 1 March 2019

Published online: 22 March 2019

References

1. Brus, L. E. Electron–electron and electron–hole interactions in small semiconductor crystallites: The size dependence of the lowest excited electronic state. *J. Chem. Phys.* **80**, 4403–4409 (1984).
2. Rossetti, R. & Brus, L. Electron-hole recombination emission as a probe of surface chemistry in aqueous cadmium sulfide colloids. *J. Phys. Chem.* **86**, 4470–4472 (1982).
3. Rossetti, R., Nakahara, S. & Brus, L. E. Quantum size effects in the redox potentials, resonance Raman spectra, and electronic spectra of CdS crystallites in aqueous solution. *J. Chem. Phys.* **79**, 1086–1088 (1983).
4. Henglein, A. Small-particle research: physicochemical properties of extremely small colloidal metal and semiconductor particles. *Chem. Rev.* **89**, 1861–1873 (1989).
5. Ekimov, A. I., Efros, A. L. & Onushchenko, A. A. Quantum size effect in semiconductor microcrystals. *Solid State Commun.* **56**, 921–924 (1985).
6. Alivisatos, A. P. Semiconductor clusters, nanocrystals, and quantum dots. *Science* **271**, 933–937 (1996).
7. Lee, S.-H. et al. Remote-type, high-color gamut white light-emitting diode based on InP quantum dot color converters. *Opt. Mater. Express* **4**, 1297–1302 (2014).
8. Nann, T. & Skinner, W. M. Quantum dots for electro-optic devices. *ACS Nano* **5**, 5291–5295 (2011).
9. Fernando, K. A. S. et al. Carbon quantum dots and applications in photocatalytic energy conversion. *ACS Appl. Mater. Interfaces* **7**, 8363–8376 (2015).

- Ma, G. Background-free in vivo time domain optical molecular imaging using colloidal quantum dots. *ACS Appl. Mater. Interfaces* **5**, 2835–2844 (2013).
- Li, L. & Reiss, P. One-pot synthesis of highly luminescent InP/ZnS nanocrystals without precursor injection. *J. Am. Chem. Soc.* **130**, 11588–11589 (2008).
- Murray, C. B., Norris, D. & Bawendi, M. G. Synthesis and characterization of nearly monodisperse CdE (E = sulfur, selenium, tellurium) semiconductor nanocrystallites. *J. Am. Chem. Soc.* **115**, 8706–8715 (1993).
- Mattoussi, H. et al. Self-assembly of CdSe–ZnS quantum dot bioconjugates using an engineered recombinant protein. *J. Am. Chem. Soc.* **122**, 12142–12150 (2000).
- Tamang, S., Lee, S., Choi, H. & Jeong, S. Tuning size and size distribution of colloidal inas nanocrystals via continuous supply of prenucleation clusters on nanocrystal seeds. *Chem. Mater.* **28**, 8119–8122 (2016).
- Tamang, S., Lincheneau, C., Hermans, Y., Jeong, S. & Reiss, P. Chemistry of InP nanocrystal syntheses. *Chem. Mater.* **28**, 2491–2506 (2016).
- Bang, E. et al. Large-scale synthesis of highly luminescent InP@ZnS quantum dots using elemental phosphorus precursor. *Chem. Mater.* **4**, 4236–4243 (2017).
- Stasiuk, G. J. et al. Cell-permeable Ln(III) chelate-functionalized InP quantum dots as multimodal imaging agents. *ACS Nano* **5**, 8193–8201 (2011).
- Lin, G. et al. In vivo toxicity assessment of non-cadmium quantum dots in BALB/c mice, *Nanomedicine Nanotechnology. Biol. Med.* **11**, 341–350 (2015).
- Brunetti, V. et al. InP/ZnS as a safer alternative to CdSe/ZnS core/shell quantum dots: in vitro and in vivo toxicity assessment. *Nanoscale* **5**, 307–317 (2013).
- Chibli, H., Carlini, L., Park, S., Dimitrijevic, N. M. & Nadeau, J. L. Cytotoxicity of InP/ZnS quantum dots related to reactive oxygen species generation. *Nanoscale* **3**, 2552–2559 (2011).
- Reiss, P., Carrière, M., Lincheneau, C., Vaure, L. & Tamang, S. Synthesis of semiconductor nanocrystals, focusing on nontoxic and earth-abundant materials. *Chem. Rev.* **116**, 10731–10819 (2016).
- Li, L., Protiere, M. & Reiss, P. Economic synthesis of high quality InP nanocrystals using calcium phosphide as the phosphorus precursor. *Chem. Mater.* **20**, 2621–2623 (2008).
- Tessier, M. D., Dupont, D., De Nolf, K., De Roo, J. & Hens, Z. Economic and size-tunable synthesis of InP/ZnE (E = S, Se) colloidal quantum dots. *Chem. Mater.* **27**, 4893–4898 (2015).
- Li, L., Reiss, P. & Protie, M. Core/shell semiconductor nanocrystals. *Small* **5**, 154–168 (2009).
- Tessier, M. D. et al. Aminophosphines: a double role in the synthesis of colloidal indium phosphide quantum dots. *J. Am. Chem. Soc.* **138**, 5923–5929 (2016).
- Shen, W. et al. Synthesis of highly fluorescent InP/ZnS small-core/thick-shell tetrahedral-shaped quantum dots for blue light-emitting diodes. *J. Mater. Chem. C* **5**, 8243–8249 (2017).
- Tamang, S., Beaune, G., Texier, I. & Reiss, P. Aqueous phase transfer of InP/ZnS nanocrystals conserving fluorescence and high colloidal stability. *ACS Nano* **5**, 9392–9402 (2011).
- Song, W. S. et al. Amine-derived synthetic approach to color-tunable InP/ZnS quantum dots with high fluorescent qualities. *J. Nanopart. Res.* **15**, 1750–1760 (2013).
- Cros-gagneux, A., Delpuch, F., Cornejo, A., Coppel, Y. & Chaudret, B. Surface chemistry of InP quantum dots: a comprehensive study. *J. Am. Chem. Soc.* **7**, 18147–18157 (2010).
- Kim, K. et al. Halide-amine Co-passivated indium phosphide colloidal quantum dots in tetrahedral shape. *Angew. Chem. Int. Ed.* **55**, 3714–3718 (2016).
- Lucey, D. W. et al. Monodispersed InP quantum dots prepared by colloidal chemistry in a noncoordinating solvent. *Chem. Mater.* **17**, 3754–3762 (2005).
- Xie, R., Kolb, U., Li, J., Basche, T. & Mews, A. Synthesis and characterization of highly luminescent CdSe–core CdS/Zn_{0.5}Cd_{0.5}S/ZnS multishell nanocrystals. *J. Am. Chem. Soc.* **127**, 7480–7488 (2005).
- Feigl, C., Russo, S. P. & Barnard, A. S. Safe, stable and effective nanotechnology: phase mapping of ZnS nanoparticles. *J. Mater. Chem.* **20**, 4971–4980 (2010).
- Ding, H., Yu, S., Wei, J. & Xiong, H. Full-color light-emitting carbon dots with a surface-state-controlled luminescence mechanism. *ACS Nano* **10**, 484–491 (2016).
- Perdew, J. P., Burke, K. & Ernzerhof, M. Generalized gradient approximation made simple. *Phys. Rev. Lett.* **77**, 3865–3868 (1996).

Acknowledgements

The authors thank Prostate Cancer UK (Grant S14-017, to J.S. and G.J.S.) and the Royal Society (Grant IE160227, to G.J.S. and S.T.) for funding this work. The work of S.C.E. was supported the U.S. Office of Naval Research through the Naval Research Laboratory's Basic Research Program. Computations were performed at the DoD Major Shared Resource Center at AFRL. S.T. thanks SERB-DST, Government of India (EMR/2016/002505) for financial support.

Author contributions

M.T.C. undertook the synthesis of the nanomaterial, photophysical studies, data analysis and paper drafting. F.N.V. measured the lifetimes and data analysis. TEM, HAADF, STEM and EDX experiments were performed by N.H. and analysed by T.C. J.S. and A.M.A. contributed to the data analysis. S.C.E. performed the density-functional theory calculations. J.-S.G.B. contributed to data analysis, explanation of results and paper writing. S.T. helped M.T.C. in some of the initial experiments on synthesis and phase transfer of QDs. S.T. and G.J.S. verified the chemical synthesis results. G.J.S. analysed data and drafted the paper. All authors contributed in the correction and proof reading of the manuscript. M.T.C., J.-S.G.B., S.T. and G.J.S. contributed to conceptualisation.

Additional information

Supplementary information accompanies this paper at <https://doi.org/10.1038/s42004-019-0138-z>.

Competing interests: The authors declare no competing interests.

Reprints and permission information is available online at <http://npg.nature.com/reprintsandpermissions/>

Publisher's note: Springer Nature remains neutral with regard to jurisdictional claims in published maps and institutional affiliations.



Open Access This article is licensed under a Creative Commons Attribution 4.0 International License, which permits use, sharing, adaptation, distribution and reproduction in any medium or format, as long as you give appropriate credit to the original author(s) and the source, provide a link to the Creative Commons license, and indicate if changes were made. The images or other third party material in this article are included in the article's Creative Commons license, unless indicated otherwise in a credit line to the material. If material is not included in the article's Creative Commons license and your intended use is not permitted by statutory regulation or exceeds the permitted use, you will need to obtain permission directly from the copyright holder. To view a copy of this license, visit <http://creativecommons.org/licenses/by/4.0/>.

© The Author(s) 2019